Optical Properties and Raman Studies of Partially Edge Terminated Vertically Aligned Nanocrystalline MoS2 Thin Film

ARTICLE · JULY 2013

Source: arXiv

Sanjeev K Gupta
Kurukshetra University

Ravindra Pandey
Michigan Technological University

Somdip Dey
Steanne Solutions Ltd, UK

Ram. S. Katiyar
University of Puerto Rico at Rio Piedras

THE JOURNAL OF PHYSICAL CHEMISTRY C

Article

pubs.acs.org/JPCC

Optical and Vibrational Studies of Partially Edge-Terminated Vertically Aligned Nanocrystalline MoS_2 Thin Films

Anand P. S. Gaur,[†] Satyaprakash Sahoo,[*,†] Majid Ahmadi,[†] Maxime J.-F. Guinel,[†,‡] Sanjeev K. Gupta,[§] Ravindra Pandey,[§] Sandwip K. Dey,[∥] and Ram S. Katiyar[*,†]

[†]Department of Physics and Institute for Functional Nanomaterials, College of Natural Sciences, and [‡]Department of Chemistry, College of Natural Sciences, University of Puerto Rico, Post Office Box 70377, San Juan, Puerto Rico 00936-8377, United States

[§]Department of Physics, Michigan Technological University, Houghton, Michigan 49931, United States

[∥]Materials Science and Engineering Program, Arizona State University, Tempe, Arizona 85287, United States

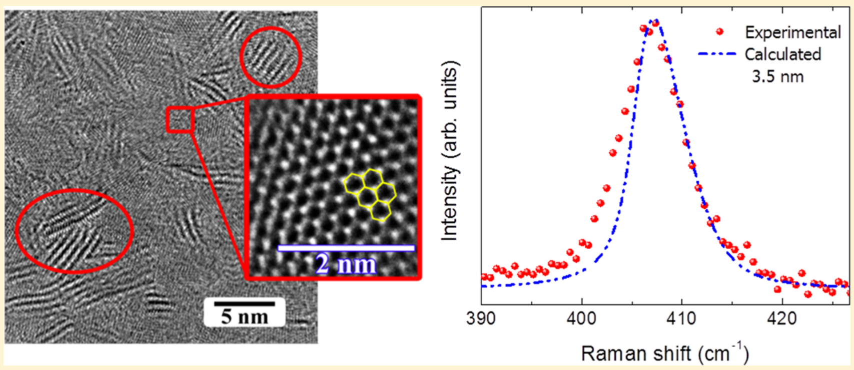

ABSTRACT: We report the optical and vibrational properties of nanocrystalline MoS_2 thin films, which are comprised of stripe-like partially edge-terminated vertically aligned (ETVA) nano-size crystals dispersed in ⟨001⟩ oriented regions, grown on large insulating substrates. From high-resolution transmission electron microscopy experiments, the average grain size of ETVA MoS_2 layers was found to be ~5 nm and consist of three to five monolayers. The ETVA and flat nanocrystalline regions were in equivalent proportions in the films. The films were highly transparent (~80%), but the transmittance decreased as the energy of the incident light approached the band gap. Additionally, weak excitonic peaks were observed in both the absorption and transmission spectra. The room-temperature Raman study showed that the line shape for both E^1_{2g} and A_{1g} modes was significantly broader, and few additional Raman modes were observed in comparison to bulk MoS_2. The broadening in the line shape of the A_{1g} mode was analyzed using the phonon-confinement model, and the calculated grain size was in good agreement with transmission electron microscopy measurements. Moreover, the temperature coefficient of the A_{1g} mode was determined from the temperature-dependent Raman studies.

■ INTRODUCTION

Two-dimensional (2D) materials are appealing for use in next-generation nanoelectronic devices. Graphene has been the most widely studied because of its superior carrier mobilities and potential for transistor applications.[1,2] However, because of the lack of bandgap of pristine graphene, the fabrication of its engineered counterpart, i.e., graphene nanoribbons and aerographite,[3] has resulted in process complexity,[4,5] reduced mobility,[6,7] and requirement of high voltages.[8,9] Therefore, a few layers or a single layer (i.e., a unit cell) of 2D transition-metal dichalcogenides or TMDs (i.e., MX_2, where transition metal, M = Mo or W and chalcogen, X = S, Se, or Te) could represent the ultimate limit of miniaturization by serving as the transistor channel material for low-power nanoelectronic devices. The prototypical TMD of molybdenum disulfide (MoS_2) is of particular interest because of its demonstrated thickness-dependent band gap and thermal and optical properties; for example, the bulk has an indirect gap of 1.2 eV, whereas a monolayer exhibits a direct gap of 1.8 eV.[10−12] Because the dimensions of monolayer MoS_2 are less than 1 nm, monolayer MoS_2-based transistors could lead to smaller and more power-efficient transistors with reduced short-channel effects.[13,14] Moreover, for optoelectronic and energy-harvesting applications that require ultrathin but transparent semiconductors, MoS_2 could complement graphene in hybrid structures.[15−17]

To date, most studies on MoS_2 have utilized free-standing or substrate-integrated layers with out-of-plane *c* axis ⟨001⟩ orientation. In one study on a few layers of MoS_2, deposited by a vapor-phase method on SiO_2/Si substrate, the in-plane E^1_{2g} and out-of-plane A_{1g} Raman modes were determined and the phonon contribution to the thermal conductivity was

Received: July 24, 2013
Revised: November 15, 2013
Published: November 20, 2013

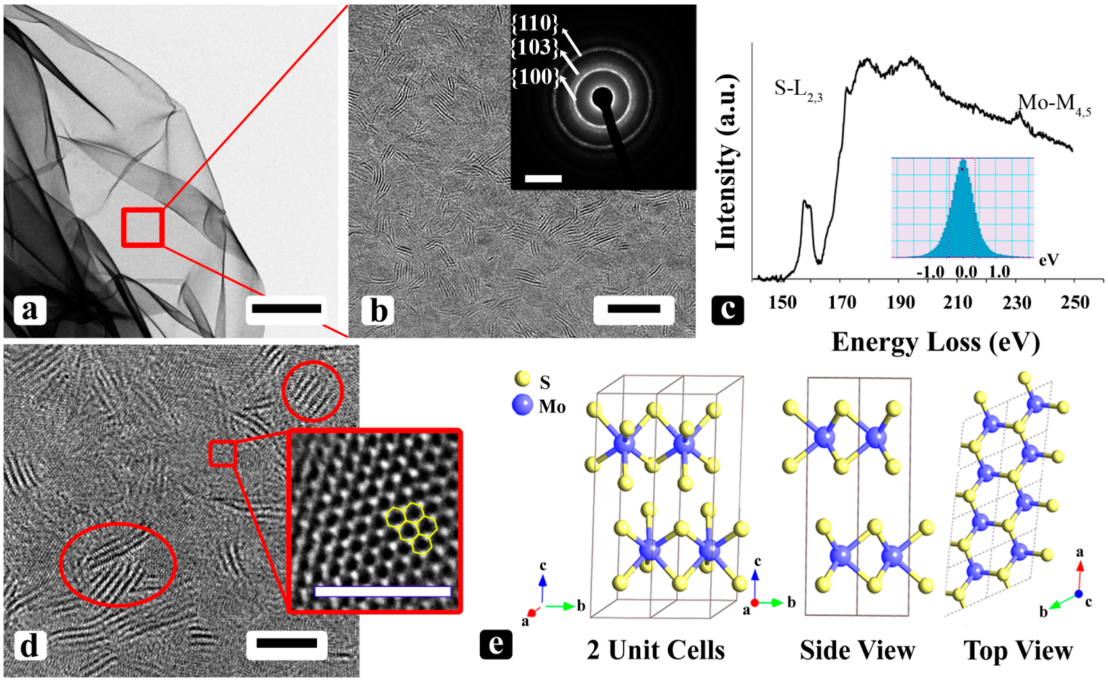

Figure 1. (a) TEM image of a suspended MoS_2 film. The scale bar is 5 nm. (b) HRTEM image of the MoS_2 film in greater detail, showing ETVA MoS_2. The scale bar is 10 nm (the inset is a SAED pattern, indexed to MoS_2). (c) EELS showing the S-$L_{2,3}$ and Mo-$M_{4,5}$ edges (resolution ~ 1 eV). (d) HRTEM images showing ETVA MoS_2 grains and ⟨001⟩-oriented grains. The scale bar is 5 nm (the inset shows a higher magnification image of hexagonal 2H-MoS_2). (e) Schematics of the 2H-MoS_2 lattice structure. The scale bars in the inset of panels b and d are 5 nm^{-1} and 2 nm, respectively.

estimated.[18] In contrast, studies on edge-terminated vertically aligned (ETVA) structures, i.e., in which ⟨001⟩ planes are perpendicular to the substrate, are rare.[19] Because the top surface or plane of an ETVA structure has dangling bonds, it may be an active plane for catalytic reactions, such as oxygen reduction and photo-oxidation of water.[20,21] Thus, ETVA MoS_2 films could be of high environmental interest because organic chemicals in air may be eliminated via the utilization of solar radiation. Therefore, for electronic or catalytic applications, the fundamental optical and vibrational properties of such materials are pertinent.

In this paper, the optical and temperature-dependent Raman scattering properties of MoS_2 layers, exhibiting a mixture of ETVA and ⟨001⟩-oriented regions are discussed. The MoS_2 layers were synthesized by the rapid sulfurization of Mo metal films on insulating substrates. The A_{1g} Raman mode was analyzed using a phonon confinement model, from which it was possible to estimate the grain size. It agreed well with measurements made from transmission electron microscopy (TEM) images. Additionally, first principles calculations were carried out to understand the absorption and phonon dispersion characteristics for bulk and single-layered MoS_2.

■ EXPERIMENTAL AND THEORETICAL METHODS

Samples were grown by the hydrosulfurization of molybdenum-coated SiO_2/Si and double-side polished (2SP) Al_2O_3 substrates using the elemental sulfur powder in a horizontal tube furnace at 550 °C for 30 min. The temperature was ramped at 10 °C/min under atmospheric pressure with a (Ar + H_2) gas mixture. Raman measurements were carried out using a Horiba-Jobin T64000 (triple mode subtractive) micro-Raman system in back-scattering geometry and a 532 nm wavelength excitation (polarized) radiation from a diode laser. The laser was focused on the sample using a 80× objective, and the laser spot size on the sample was about 1 μm. We had used low laser power (0.5 mW) to avoid any laser heating of the sample. The MoS_2 samples were transferred to conventional copper TEM grids and characterized using a high-resolution TEM (HRTEM; JEOL JEM-2200FS).

Theoretical calculations were performed to simulate the electronic band structure of bulk, monolayer, and nanocrystalline MoS_2. Here, the Quantum Espresso code employed the local density approximation (LDA), via the adoption of the exchange-correlation function by Perdew and Wang, to density functional theory.[22,23] An ultrasoft pseudo-potential description of the electron−electron interaction was used with valence electrons $4d^5$, $5s^1$ and $3s^2$, $3p^4$ of Mo and S atoms, respectively. A plane-wave basis set for the electronic wave functions and the charge density was applied, with kinetic energy cutoffs set to 50 and 500 Ry, respectively. For the monolayer, the periodic boundary condition of the separation between neighboring cells in the (xy) plane was a distance of 20 Å. The configurations using the criteria of forces and stresses on atoms were relaxed until the energy change was less than 10^{-4} eV. For the geometry optimization, the internal coordinates were relaxed until the Hellmann−Feynman forces were within 0.01 eV/Å. Additionally, phonon calculations for the MoS_2 bulk were performed by density functional perturbation theory (DFPT) with a fixed occupation scheme for electronic excitation.[24] A 11 × 11 × 1 Monkhorst−Pack (MP) k-mesh was found to yield phonon frequencies converged to within 4 cm^{-1}, and 5 × 5 × 1 q-mesh in the first Brillouin zone (BZ) was used in the interpolation of the force constants for the phonon dispersion calculations. Convergence limit of phonon calculation was also tested for higher mesh and cutoff energy and found that the phonon frequencies converged up to 4 cm^{-1}. The phonon

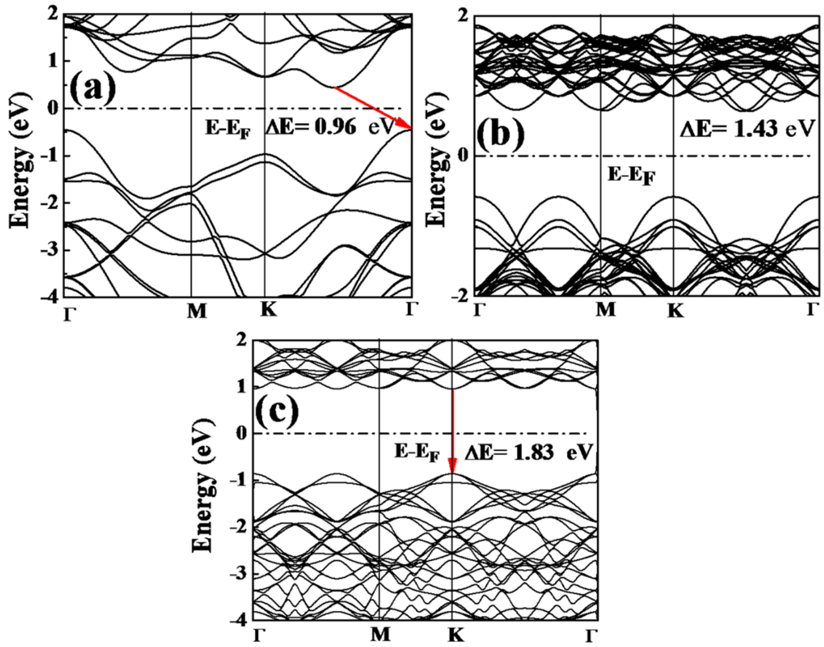

Figure 2. Calculated band structure of (a) bulk, (b) nanocrystalline, and (c) monolayer MoS_2.

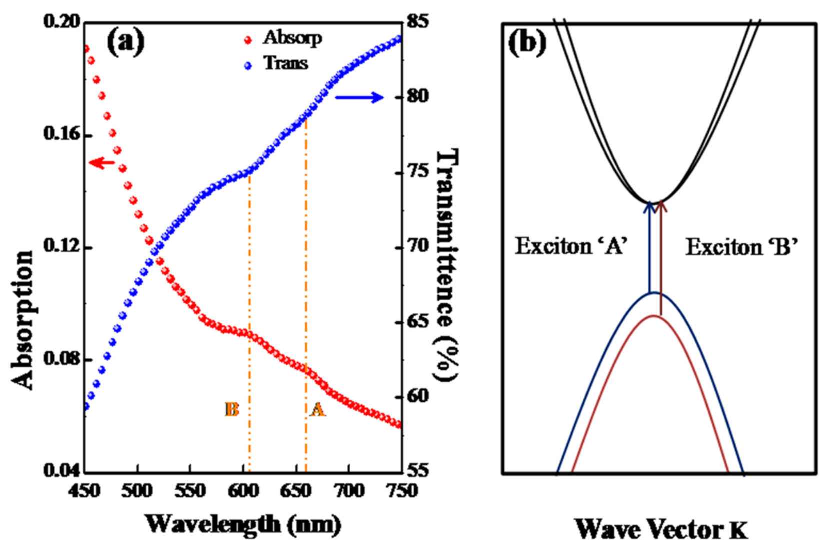

Figure 3. (a) Absorption and transmission spectra of the partially ETVA MoS_2 thin film. (b) Schematic representation of A and B excitonic transitions.

density of states were calculated using a 11 × 11 × 1 *k*-point mesh and was found to yield convergent results.

■ RESULTS AND DISCUSSION

Figure 1a is a bright-field TEM image of a large, free-standing MoS_2 film. Figure 1b shows a HRTEM image of the same film, where the inset is a typical selected area electron diffraction (SAED) pattern, indexed to hexagonal MoS_2 [Joint Committee on Powder Diffraction Standards (JCPDS) card number 73-1508]. The unique structure of this film is a mixture of ETVA MoS_2 grains and ⟨001⟩-oriented layers of MoS_2, in similar proportions. Note that the overall film is flat, and partially ETVA grains do not protrude from the film, with average thickness and lateral width of the ETVA regions of about 5 and 6 nm, respectively. Electron energy loss spectra (EELS) were recorded from the same film using the in-column energy filter that equipped the 2200FS instrument. The spectrum displayed in Figure 1c shows the S-$L_{2,3}$ and Mo-$M_{4,5}$ edges located at 165 and 227 eV, respectively. The resolution was approximately 1 eV, as illustrated with the zero loss peak (inset). A HRTEM image showing ETVA grains is displayed in Figure 1d. The inset is a higher magnification image of ⟨001⟩-oriented layers. It compares well to the structure of 2H-MoS_2, for which schematics of the unit cell and views along two directions are displayed in Figure 1e.

The calculated electronic band structures at the level of local density approximation−density functional theory (LDA−DFT) approximation along the high-symmetry directions in the BZ are shown in panels a, b, and c of Figure 2 for the bulk, nanocrystal, and monolayer of MoS_2, respectively. For bulk MoS_2, an indirect band gap (0.96 eV) was observed, whereas for the MoS_2 monolayer, a direct band gap (1.83 eV) was observed; the direct excitonic transition energy at the BZ *k* point changes with the layer thickness and becomes so high in a monolayer that it changes to direct bandgap material. Here, the band structure of MoS_2 grains[25] of dimension 9.4 Å also shows a direct band gap but with a magnitude of ∼1.43 eV. The calculated band gap is in good agreement with reported experimental results.[9]

The optical properties of the partially ETVA MoS_2 film are shown in Figure 3a. The film is quite transparent for light of lower energies than the band gap of MoS_2. There are two peaks in both the absorption and transmission spectra. These peaks are indicated by two dash-dot lines (A and B) on the plot. These are reported to be the excitonic transitions at the BZ k point in bulk MoS_2 (Figure 3b) appearing at 610 and 675 nm and denoted as A and B transitions, respectively.[26,27] The energy difference between these two transitions is about 0.12 eV, and this is due to the spin−orbital splitting of the valence band.[11,28] Note that, in the case of bulk MoS_2, these peaks are quite strong and sharp, whereas for thin films, they are considerably weaker. The observed low intensities of these peaks could be due to the relatively lower population of exciton. Although the current DFT calculations show that direct excitonic transitions remain unchanged with a decreasing number of layers, the band gap, however, shifts from indirect to direct in the case of single-layer MoS_2 (Figure 2b).

In the following paragraphs, focus is on the phonon properties of the MoS_2 bulk. Figure 4 presents the phonon dispersion curves along with the phonon density of states for MoS_2 bulk. Because there are 6 atoms per unit cell, one expects 18 (3 acoustic and 15 optical) phonon branches as MoS_2. However, 12 phonon branches have been observed in the neutron diffraction experiment by Wakabayashi et al., 2 acoustic and 10 optical phonons. This indicates 1 acoustic and 5 optical modes are doubly degenerated. The longitudinal acoustic and transverse acoustic modes have linear dispersion where as the out-of-plane acoustic mode has q^2 dependence and this could be due to point-group symmetry as seen in graphene.[29] The overall agreement between theory and experiment[30] is good, even for the interlayer modes. This confirms our expectation that the LDA−DFT approximation describes reasonably well the interlayer interaction. The low-frequency optical modes in MoS_2 correspond to shear mode which are in analogy with graphite.[31] The phonon dispersion relations along with the phonon density of states possess two distinct regions. The highest vibrational modes are due to S atoms, whereas the vibrations of the Mo atoms play the most prominent role for the lowest modes. There is a large difference between the frequencies of highest and lowest level vibration modes because of the large mass ratio between Mo and S atoms. The high-frequency optical modes are separated from the low-frequency modes by a gap of ∼50 cm^{-1}.

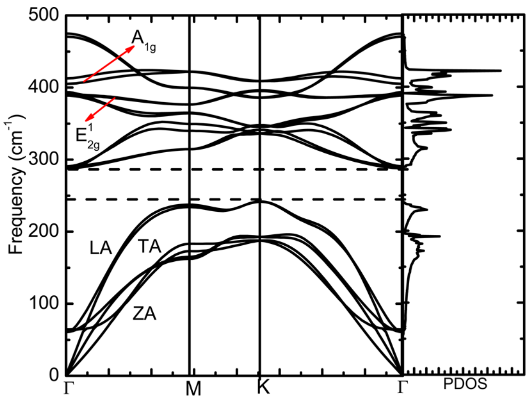

Figure 4. Calculated phonon dispersion and the phonon density of states of bulk MoS_2.

For layered materials, Raman spectroscopy has been employed very efficiently to determine the number of layers (using the band position and intensity), the mechanical properties, and the thermal properties.[18,32] Moreover, it is possible to determine the grain size in the sub-nanometer range decisively.[33] In the following section, we present comparative Raman studies of the bulk and partially ETVA MoS_2 thin film at room temperature. Hexagonal MoS_2 belongs to space group D_{6h} ($P6_3/mmc$), for which zone-center Raman- and infrared (IR)-active vibrational modes are presented in the following irreducible decomposition:[34] $\Gamma = A_{1g} + E_{1g} + 2E^1_{2g} + 2E^2_{2g} + E_{1u} + A_{2u}$, where A_{1g} (409 cm^{-1} out-of-plane breathing mode), E^2_{2g} (32 cm^{-1} interlayer vibration), E_{1g} (287 cm^{-1} in-plane vibration), and E^1_{2g} (383 cm^{-1} in-plane vibration) modes are Raman-active, while the other two are IR-active. Interestingly, E_{1u} and E^1_{2g} modes are degenerated (provided that the van der Waals interaction between the layers is very weak), and the only difference is that they vibrate in the 180° interlayer phase shift.[35] Figure 5 shows the room-temperature first-order Raman spectra of the bulk (SPI, West Chester, PA) and partially ETVA thin film of MoS_2.

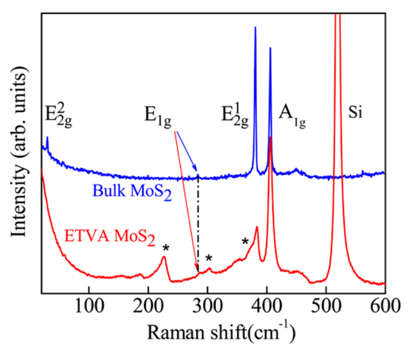

Figure 5. Comparison of the room-temperature Raman spectra of the bulk MoS_2 and partially ETVA MoS_2 thin film. The Si substrate peak is at 521 cm^{-1}.

Zone-center Raman bands were observed in both the bulk and partially ETVA MoS_2 thin film at 31, 287, 383, and 407 cm^{-1} and are assigned to E^2_{2g}, E_{1g}, E^1_{2g}, and A_{1g} modes, respectively. We also observed a clear broadening of the intense E^1_{2g} and A_{1g} modes in the partially ETVA MoS_2 thin film. Second, few weak additional peaks were found at about 225, 300, and 375 cm^{-1} for partially ETVA MoS_2 films (marked with an asterisk in Figure 5). The origin of these peaks is associated with the zone boundary phonons, and similar results were recently observed by Chakraborty et al.[36] The Raman band positions match with some of the zone boundary (M or K-symmetry points) of the phonon dispersion curve shown in Figure 4. Similar results were reported for pulsed laser deposition (PLD)-grown MoS_2 films at room temperature, where they found that the disorder peak disappears with annealing of the sample.[37] Similar results were reported by Yang et al., where the low-frequency band was assigned to octahedral MoS_2, which is considered a metastable decaying phase.[38]

Now a discussion on the line shape asymmetry of the A_{1g} mode is in order. This mode was chosen because the peak shape is well-defined. In bulk MoS_2, the full width at half-maximum (fwhm) for the A_{1g} mode is $\sim 3\ cm^{-1}$, whereas its value is about 3 times higher for the partially ETVA MoS_2 sample. In bulk materials, the zone-center optical phonon ($q = 0$) only contributes to the phonon line shape in Raman spectra. However, as the size of the material decreases significantly and falls in the range of the sub-nanometer scale, the phonons with $q \neq 0$ also start contributing to the line shape in the dispersion curve. The Raman selection rule ($q = 0$) relaxes in such cases, which leads to a shift and asymmetric broadening of the line shape. The phonon confinement model, initially proposed by Richeter et al., which was later modified by Campbell and Fauchet for nanomaterials of different geometries, explains such size-dependent Raman spectra.[39,40] This might be useful to explain the Raman line broadening that appeared in vertically oriented stripe-like grains of MoS_2 films.

This model considers the contribution of phonons away from the zone center by integrating over the entire BZ to obtain the Raman line shape, and the phonon amplitude is taken as an exponentially decay function. For a given nanoparticle size d, the Gaussian confinement function is used, which is given by

$$W(r) = \exp\left(\frac{-\alpha r^2}{d^2}\right) \tag{1}$$

where the magnitude of α determines how fast the wave function decays as one approaches the boundary. In this calculation, $\alpha = 8\pi^2$. The Fourier transformation of the confinement function is the weight factor that estimates the contribution of phonons other than the zone center. The weight factor in this case is

$$|C(q)|^2 = \exp\left(\frac{-q^2 d^2}{2\alpha}\right) \tag{2}$$

The Raman line intensity was calculated by integrating these contributions over the complete BZ, which can be given by

$$I(\omega) = \int \frac{|C(q)|^2}{[\omega - \omega(q)]^2 + \left(\frac{\Gamma_0}{2}\right)^2} d^3q \tag{3}$$

where Γ_0 and $\omega(q)$ are the natural line width and the phonon dispersion curve of the zone-center optical phonon in bulk MoS_2. Figure 6a shows the calculated phonon line shape of A_{1g} mode for two nanoparticle sizes (2 and 3.5 nm) using the phonon confinement model. It may be pointed out that, as the particle size decreases, the calculated Raman line shape broadens significantly. The observed line shape is fitted best with 3.5 nm grain size (Figure 6b), which is in very good accordance with TEM results (the average grain size was measured to be less than 5 nm). However, the fitted line shape does not fit well in the low-frequency side of the experimental spectrum; the low-frequency side of the experimental spectrum is broader.

This section discusses the disagreement of the experimental line shape from the phonon confinement model. We first consider the microscopic factors affecting the phonon line shape in bulk material and given by Matthiessen's rule: $(1/\tau) = (1/\tau_u) + (1/\tau_b) + (1/\tau_m) + (1/\tau_{e-ph})$, where the terms on the right side denote the inverse of the lifetime of different

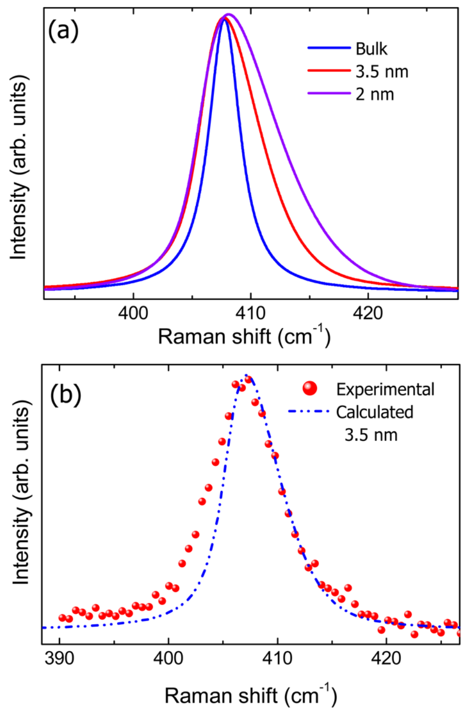

Figure 6. (a) Calculated phonon line shape for the A_{1g} mode for two nanoparticle sizes using the phonon confinement model. (b) Comparison of the experimental Raman spectrum and the calculated phonon line shape with a particle size of 3.5 nm.

microscopic processes and contribute to the phonon line shape via the Umklapp process, boundary, mass difference, and electron phonon scattering, respectively.[41] This is due to the fact that the phonon confinement model does not take these factors into account. In the present work, Umpklapp scattering is not significant because the experiments were performed at room temperature. Similarly, the presence of isotopes in our sample can be neglected, hence, mass difference contributions to the Raman line shape. However, the isotope effect on the Raman line shape has been observed in graphene. The other two remaining scattering processes can significantly affect the Raman line shape, especially in grains. Apart from the conventional boundary scattering, the defects in grains can act as scattering centers and contribute to the Raman line shape.

Recently, we have demonstrated the temperature-dependent Raman studies to understand the lattice anharmonicity in the high-quality large-scale few-layer MoS_2 thin film. It is also appropriate to investigate the lattice anharmonicity in the ETVA MoS_2 film. Thus, we performed temperature-dependent Raman studies in the temperature range of 83−423 K. Higher temperatures were not considered because they could damage it. Figure 7a shows the A_{1g} and E^1_{2g} modes in this temperature range. A blue shift in the peak position of the A_{1g} mode was observed as the temperature was decreased. Surprisingly, a new peak (marked with an asterisk in Figure 7a) at about 373 cm^{-1} was observed at the low-energy side of the E^1_{2g} mode. This was not observed for high-quality few-layer MoS_2. Sekine et al. has observed a similar trend for bulk MoS_2 by tuning the laser excitation energy across the A and B excitonic levels.[42] The new peak associated with the E^1_{2g} mode at low temperatures was assigned to the E^2_{1u} mode, which is a Raman-inactive mode. This peak appears because of the resonance effect, and the

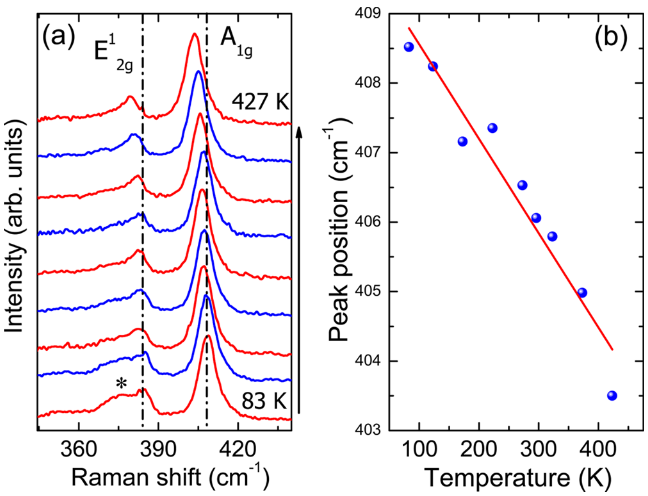

Figure 7. (a) Temperature-dependent Raman spectra for the partially ETVA MoS_2 thin film. (b) Plot of the temperature versus the A_{1g} peak position.

small frequency splitting of the Davydov pair (E^2_{1u} and E^1_{2g}) is caused by a very weak interlayer interaction. Figure 7b shows the plot of the A_{1g} mode peak position as a function of the temperature. The data were fitted using the linear equation $\omega(T) = \omega_0 + \chi T$, where ω_o is the vibrational frequency at absolute zero temperature and χ is the first-order temperature coefficient of A_{1g} mode. The fitted numerical value of χ (-1.36×10^{-2}) matches well with the bulk MoS_2.

■ CONCLUSION

In conclusion, large-scale nanocrystalline thin films of MoS_2, comprised of a mixture of partially ETVA and flat (⟨001⟩-oriented) regions, were synthesized and analyzed using Raman spectroscopy and TEM. The theoretically calculated band structure revealed that, with a decrease in the number of layers, the band gap of MoS_2 increased. From the room-temperature Raman spectroscopic studies, it was observed that E^1_{2g} and A_{1g} peaks in partially ETVA MoS_2 are significantly broader than those of bulk MoS_2, and this broadening has been attributed to phonon confinement. The Raman line broadening of the A_{1g} mode was analyzed using the phonon confinement model, and the calculated grain size was found to be in good agreement with TEM results. The calculated Raman line shape did not match well to the data, and the extra broadening was attributed to conventional boundary scattering and the defects in grains.

■ AUTHOR INFORMATION

Corresponding Authors

*Telephone: 1-787-751-4210. E-mail: satya504@gmail.com.
*Telephone: 1-787-751-4210. E-mail: rkatiyar@hpcf.upr.edu.

Notes

The authors declare no competing financial interest.

■ ACKNOWLEDGMENTS

The authors acknowledge financial support from the U.S. Department of Energy (DOE) (Grant DE-FG02-08ER46526). Anand P. S. Gaur is thankful for the National Science Foundation (NSF) fellowship (Grant NSF-RII-1002410).

■ REFERENCES

(1) Novoselov, K. S.; Geim, A. K.; Morozov, S. V.; Jiang, D.; Zhang, Y.; Dubonos, S. V.; Grigorieva, I. V.; Firsov, A. A. Electric field effect in atomically thin carbon films. *Science* **2004**, *306*, 666−669.

(2) Berger, C.; Song, Z.; Li, T.; Li, X.; Ogbazghi, A. Y.; Feng, R.; Dai, Z.; Marchenkov, A. N.; Conrad, E. H.; First, P. N.; et al. Ultrathin epitaxial graphite: 2D electron gas properties and a route toward graphene-based nanoelectronics. *J. Phys. Chem. B* **2004**, *108*, 19912−19916.

(3) Mecklenburg, M.; Schuchardt, A.; Mishra, Y. K.; Kaps, S.; Adelung, R.; Lotnyk, A.; Kienle, L.; Schulte, K. Aerographite: Ultra lightweight, flexible nanowall, carbon microtube material with outstanding mechanical performance. *Adv. Mater.* **2012**, *24*, 3486−3490.

(4) Han, M. Y.; Özyilmaz, B.; Zhang, Y.; Kim, P. Energy band-gap engineering of graphene nanoribbons. *Phys. Rev. Lett.* **2007**, *98*, 206805.

(5) Li, X.; Wang, X.; Zhang, L.; Lee, S.; Dai, H. Chemically derived, ultrasmooth graphene nanoribbon semiconductors. *Science* **2008**, *319*, 1229−1232.

(6) Yoon, Y.; Guo, J. Effect of edge roughness in graphene nanoribbon transistors. *Appl. Phys. Lett.* **2007**, *91*, 073103.

(7) Obradovic, B.; Kotlyar, R.; Heinz, F.; Matagne, P.; Rakshit, T.; Giles, M. D.; Stettler, M. A.; Nikonov, D. E. Analysis of graphene nanoribbons as a channel material for field-effect transistors. *Appl. Phys. Lett.* **2006**, *88*, 142102.

(8) Zhang, Y. B.; Tang, T. T.; Girit, C.; Hao, Z.; Martin, M. C.; Zettl, A.; Crommie, M. F.; Shen, Y. R.; Wang, F. Direct observation of a widely tunable bandgap in bilayer graphene. *Nature* **2009**, *459*, 820−823.

(9) Xia, F.; Farmer, D. B.; Lin, Y.-m.; Avouris, P. Graphene field-effect transistors with high on/off current ratio and large transport band gap at room temperature. *Nano Lett.* **2010**, *10*, 715−718.

(10) Mak, K. F.; Lee, C.; Hone, J.; Shan, J.; Heinz, T. F. Atomically thin MoS_2: A new direct-gap semiconductor. *Phys. Rev. Lett.* **2010**, *105*, 136805.

(11) Splendiani, A.; Sun, L.; Zhang, Y.; Li, T.; Kim, J.; Chim, C.-Y.; Galli, G.; Wang, F. Emerging photoluminescence in monolayer MoS_2. *Nano Lett.* **2010**, *10*, 1271−1275.

(12) Cao, T.; Wang, G.; Han, W. P.; Ye, H. Q.; Zhu, C. R.; Shi, J. R.; Niu, Q.; Tan, P. H.; Wang, E.; Liu, B. L. Valley-selective circular dichroism of monolayer molybdenum disulphide. *Nat. Commun.* **2012**, *3*, No. 887.

(13) Wang, H.; Yu, L.; Lee, Y.-H.; Shi, Y.; Hsu, A.; Chin, M. L.; Li, L.-J.; Dubey, M.; Kong, J.; et al. Integrated circuits based on bilayer MoS_2 transistors. *Nano Lett.* **2012**, *12*, 4674−4680.

(14) Wang, Q. H.; Kalantar-Zadeh, K.; Kis, A.; Coleman, J. N.; Strano, M. S. Electronics and optoelectronics of two-dimensional transition metal dichalcogenides. *Nat. Nanotechnol.* **2012**, *7*, 699−712.

(15) Radisavljevic, B.; Whitwick, M. B.; Kis, A. Integrated circuits and logic operations based on single-layer MoS_2. *ACS Nano* **2011**, *5*, 9934−9938.

(16) Shi, Y.; Zhou, W.; Lu, A.-Y.; Fang, W.; Lee, Y.-H.; Hsu, A. L.; Kim, S. M.; Kim, K. K.; Yang, H. Y.; Li, L.-J.; et al. van der Waals epitaxy of MoS_2 layers using graphene as growth templates. *Nano Lett.* **2012**, *12*, 2784−2791.

(17) Lee, H. S.; Min, S.-W.; Chang, Y.-G.; Park, M. K.; Nam, T.; Kim, H.; Kim, J. H.; Ryu, S.; Im, S. MoS_2 nanosheet phototransistors with thickness-modulated optical energy gap. *Nano Lett.* **2012**, *12*, 3695−3700.

(18) Sahoo, S.; Gaur, A. P. S.; Ahmadi, M.; Guinel, M. J. F.; Katiyar, R. S. Temperature-dependent Raman studies and thermal conductivity of few-layer MoS_2. *J. Phys. Chem. C* **2013**, *117*, 9042−9047.

(19) Kong, D.; Wang, H.; Cha, J. J.; Pasta, M.; Koski, K. J.; Yao, J.; Cui, Y. Synthesis of MoS_2 and $MoSe_2$ films with vertically aligned layers. *Nano Lett.* **2013**, *13*, 1341−1347.

(20) Hinnemann, B.; Moses, P. G.; Bonde, J.; Jørgensen, K. P.; Nielsen, J. H.; Horch, S.; Chorkendorff, I.; Nørskov, J. K. Biomimetic

hydrogen evolution: MoS_2 nanoparticles as catalyst for hydrogen evolution. *J. Am. Chem. Soc.* **2005**, *127*, 5308−5309.

(21) Jaramillo, T. F.; Jørgensen, K. P.; Bonde, J.; Nielsen, J. H.; Horch, S.; Chorkendorff, I. Identification of active edge sites for electrochemical H_2 evolution from MoS_2 nanocatalysts. *Science* **2007**, *317*, 100−102.

(22) http://www.pwscf.org.

(23) Perdew, J. P.; Chevary, J. A.; Vosko, S. H.; Jackson, K. A.; Pederson, M. R.; Singh, D. J.; Fiolhais, C. Atoms, molecules, solids, and surfaces: Applications of the generalized gradient approximation for exchange and correlation. *Phys. Rev. B: Condens. Matter Mater. Phys.* **1992**, *46*, 6671−6687.

(24) Giannozzi, P.; Baroni, S.; Bonini, N.; Calandra, M.; Car, R.; Cavazzoni, C.; Ceresoli, D.; Chiarotti, G. L.; Cococcioni, M.; Dabo, I.; et al. QUANTUM ESPRESSO: A modular and open-source software project for quantum simulations of materials. *J. Phys.: Condens. Matter* **2009**, *21*, 395502−395519.

(25) Li, T.; Galli, G. Electronic properties of MoS_2 nanoparticles. *J. Phys. Chem. C* **2007**, *111*, 16192−16196.

(26) Coehoorn, R.; Haas, C.; de Groot, R. A. Electronic structure of $MoSe_2$, MoS_2, and WSe_2. II. The nature of the optical band gaps. *Phys. Rev. B: Condens. Matter Mater. Phys.* **1987**, *35*, 6203−6206.

(27) Böker, T.; Severin, R.; Müller, A.; Janowitz, C.; Manzke, R.; Voß, D.; Krüger, P.; Mazur, A.; Pollmann, J. Band structure of MoS_2, $MoSe_2$, and α-$MoTe_2$: Angle-resolved photoelectron spectroscopy and ab initio calculations. *Phys. Rev. B: Condens. Matter Mater. Phys.* **2001**, *64*, 235305−235310.

(28) Frey, G. L.; Elani, S.; Homyonfer, M.; Feldman, Y.; Tenne, R. Optical-absorption spectra of inorganic fullerenelike MS_2 (M = Mo, W). *Phys. Rev. B: Condens. Matter Mater. Phys.* **1998**, *57*, 6666−6671.

(29) Graf, D.; Molitor, F.; Ensslin, K.; Stampfer, C.; Jungen, A.; Hierold, C.; Wirtz, L. Spatially resolved Raman spectroscopy of single- and few-layer graphene. *Nano Lett.* **2007**, *7*, 238−242.

(30) Wakabayashi, N.; Smith, H. G.; Nicklow, R. M. Lattice dynamics of hexagonal MoS_2 studied by neutron scattering. *Phys. Rev. B: Condens. Matter Mater. Phys.* **1975**, *12*, 659−663.

(31) Lee, C.; Yan, H.; Brus, L. E.; Heinz, T. F.; Hone, J.; Ryu, S. Anomalous lattice vibrations of single- and few-layer MoS_2. *ACS Nano* **2010**, *4*, 2695−2700.

(32) Sahoo, S.; Arora, A. K.; Sridharan, V. Raman line shapes of optical phonons of different symmetries in anatase TiO_2 nanocrystals. *J. Phys. Chem. C* **2009**, *113*, 16927−16933.

(33) Spanier, J. E.; Robinson, R. D.; Zhang, F.; Chan, S.-W.; Herman, I. P. Size-dependent properties of CeO_{2-y} nanoparticles as studied by Raman scattering. *Phys. Rev. B: Condens. Matter Mater. Phys.* **2001**, *64*, 245407−245408.

(34) Wieting, T. J.; Verble, J. L. Infrared and Raman studies of long-wavelength optical phonons in hexagonal MoS_2. *Phys. Rev. B: Condens. Matter Mater. Phys.* **1971**, *3*, 4286−4292.

(35) Verble, J. L.; Wieting, T. J. Lattice mode degeneracy in MoS_2 and other layer compounds. *Phys. Rev. Lett.* **1970**, *25*, 362−365.

(36) Chakraborty, B.; Matte, H. S. S. R.; Sood, A. K.; Rao, C. N. R. Layer-dependent resonant Raman scattering of a few layer MoS_2. *J. Raman Spectrosc.* **2013**, *44*, 92−96.

(37) Mcdevitt, N. T.; Zabinski, J. S.; Donley, M. S.; Bultman, J. E. Disorder-induced low-frequency Raman band observed in deposited MoS_2 films. *Appl. Spectrosc.* **1994**, *48*, 733−736.

(38) Yang, D.; Sandoval, S. J.; Divigalpitiya, W. M. R.; Irwin, J. C.; Frindt, R. F. Structure of single-molecular-layer MoS_2. *Phy. Rev. B: Condens. Matter Mater. Phys.* **1991**, *43*, 12053−12056.

(39) Campbell, I. H.; Fauchet, P. M. The effects of microcrystal size and shape on the one phonon Raman spectra of crystalline semiconductors. *Solid State Commun.* **1986**, *58*, 739−741.

(40) Richter, H.; Wang, Z. P.; Ley, L. The one phonon Raman spectrum in microcrystalline silicon. *Solid State Commun.* **1981**, *39*, 625−629.

(41) Matthiessen, A.; Vogt, C. On the influence of temperature on the electric conducting-power of alloys. *Phil. Trans. R. Soc. London* **1864**, *154*, 167−200.

(42) Sekine, T.; Uchinokura, K.; Nakashizu, T.; Matsuura, E.; Yoshizaki, R. Dispersive Raman mode of layered compound 2H-MoS_2 under the resonant condition. *J. Phys. Soc. Jpn.* **1984**, *53*, 811−818.